

Feasibility of a Multi-Pass Thomson Scattering System with Confocal Spherical Mirrors

Junichi HIRATSUKA, Akira EJIRI, Yuichi TAKASE and Takashi YAMAGUCHI

The University of Tokyo, Kashiwa 277-8561, Japan

(Received 12 April 2010 / Accepted 27 August 2010)

Multi-pass Thomson scattering is an attractive method for measuring electron temperature and density in low density plasmas. The feasibility of multi-pass laser optics consisting of two confocal spherical mirrors has been studied, and analytic expressions for the path have been obtained. These can be used to optimize the design under the given conditions. The effects of aberration, as well as positioning and alignment errors, were found to be critical for obtaining large transit numbers. Beam expansion resulting from aberration, surface roughness of the mirrors and diffraction is considered. Under practical conditions, transit numbers of about 37 (i.e., 19 round trips) are possible.

© 2010 The Japan Society of Plasma Science and Nuclear Fusion Research

Keywords: Thomson scattering, multi-pass, confocal mirror, ECH start-up, low-density plasma

DOI: 10.1585/pfr.5.044

Multi-pass Thomson scattering has the advantage of enhancing the scattered signal by accumulating signals from multiple passes through the plasma. On the TST-2 spherical tokamak device, non inductive start-up experiments were conducted using ECH (2.45 GHz/5 kW) [1]. According to interferometric measurements, typical electron densities are $n_e \sim 10^{17} \text{ m}^{-3}$, about two orders of magnitude lower than typical densities in ohmic discharges. Therefore, enhancement of the scattered signal by a multi-pass scheme is necessary.

On TEXTOR, multi-pass measurements were carried out using two spherical mirrors. The mirrors can be aligned for different number of passes, such as double- and six-pass. In this six-pass system, the laser beam passes through the plasma six times and returns to the laser rod. Compared with the double-pass system on TEXTOR, the pulse probing energy was increased by a factor of 2.6 and the total probing energy during each 9 ms pumping pulse was increased by a factor of 4. In this system, the angles of the mirrors must be aligned with a precision of $\sim 10^{-5} \text{ rad}$ [2]. Although their achievement is remarkable, it uses an intracavity configuration in which the mirrors for the multi-pass system enclose a laser cavity and the laser oscillates along the scattering path. Such a scheme may not be useful for devices in which the laser system is independent from the rest of the optical system. Furthermore, the dependence of the pass and transit numbers on the optical parameters and the theoretical limits of multi-pass optics have not been clarified. In this paper, theoretical aspects of the confocal mirror system are studied. General expressions for the beam path and transit number of a confocal spherical mirror system are obtained for a general configuration.

Several schemes are possible for multi-pass optics. (i) The first is coaxial confinement using a fast gate such as a Pockels cell. By switching the Pockels cell, the laser polarization can be changed. Laser light can be confined by combining a Pockels cell and a polarizer. An advantage of this scheme is that the alignment procedure is simple because the optical axis is unique. (ii) A system with two parallel mirrors is the simplest. While laser light travels between the two mirrors, the reflection point moves slowly along each mirror. Since the beam axis moves, the maximum transit number is determined by the allowable motion of the axis. (iii) A confocal spherical mirror system is as simple as a two parallel mirror system, but the beam paths tend to converge to the axis of the mirrors, and a large transit number is assumed to be possible. This paper presents the results of a theoretical analysis of the confocal mirror system, particularly the maximum transit number. The beam path is formulated analytically. In addition, the effects of positioning and alignment errors are formulated.

A confocal mirror system consists of two concave mirrors with a common focal point and a common axis (Fig. 1). Incident light parallel to the mirror axis is reflected by the first mirror (at height $z_1 > 0$), passes through the focal point, and hits the second mirror (at height $z_2 < 0$). The light is reflected by the second mirror, becomes parallel to the mirror axis, and hits the first mirror (at height $z_3 < 0$). This process is repeated, and the light gradually approaches the mirror axis. How it approaches the axis depends on the focal lengths of the two mirrors. When parabolic mirrors are used, the light converges to the axis; whereas in the case of spherical mirrors, the light deviates from the axis after a certain number of transits because of aberration. In general, the surface accuracy of parabolic mirrors is not as good as that of spherical mirrors. More-

author's e-mail: hiratsuka@fusion.k.u-tokyo.ac.jp

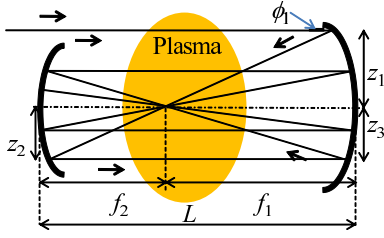


Fig. 1 Schematic drawing of a confocal spherical mirror system. Important variables are defined in the figure.

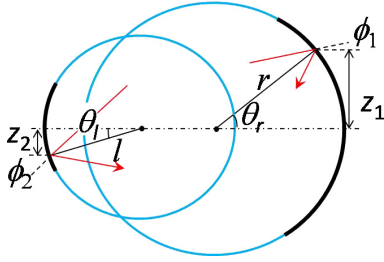


Fig. 2 Definitions of the injection angles ϕ_1 and ϕ_2 and hit positions z_1 , z_2 and θ_r , θ_l .

over, spherical mirrors with various focal lengths are readily available. Therefore, in this paper, we study confocal mirror systems consisting of spherical mirrors. In addition to aberration, we need to consider the accuracy of alignment and positioning. Note that a parabolic mirror has a unique optical axis, whereas the optical axis of a spherical mirror is not unique. Therefore, the alignment is much more difficult for parabolic mirrors than that for spherical mirrors.

The system is identified by the following five variables: injection angle ϕ_1 ; hit position z_1 on the first mirror; focal lengths f_1 , f_2 ($f_1 \geq f_2$); and the distance between the mirrors L . The radii of curvature for the mirrors are $r = 2f_1$ and $l = 2f_2$ (Fig. 2). The angles $\theta_r = \arctan(z_1/r)$ and $\theta_l = \arctan(-z_2/l)$ determine the hit points. The incident condition (i.e., the initial condition) is defined by the incident angle $\phi \equiv \phi_1$ and the normalized first hit point $z \equiv z_1/r$. In the following, we assume $z \ll 1$, because z_1 is smaller than the window radius and r and l are larger than the diameter of the device. In particular, z_1 is several tens of millimeters, whereas r and l are several meters. We derive analytic expressions to determine the path as a function of ϕ and z . In the derivation, we keep terms up to $O(z^3)$ and neglect the higher-order terms. We assume $\phi = O(z^3)$.

The angle of the reflected light ϕ_2 from the first mirror is

$$\phi_2 = 2\theta_r - \phi_1 \approx 2z + \frac{z^3}{3} - \phi. \quad (1)$$

Here, we use the approximation $\theta_r \sim z + z^3/6$. Since the mirrors have a finite thickness, the distance between the two hit points differs from L by about $(z_1^2/r + z_2^2/l)/2$.

The difference is $O(z^2) \times L$. Using the distance between the two hit points and ϕ_2 , the position of the second hit point is

$$\hat{z}_2 = -\frac{l}{r}z - \frac{L}{r}z^3 + \frac{L}{r}\phi. \quad (2)$$

Here, $\hat{z}_i \equiv z_i/r$ is the normalized i -th hit point. In the same manner,

$$\phi_3 = 2\theta_l - \phi_2 \approx \left(1 + \frac{r}{l}\right)z^3 - \frac{r}{l}\phi, \quad (3)$$

$$\hat{z}_3 = -\frac{l}{r}z + \frac{1}{2}\left(1 + \frac{r}{l}\right)z^3 + \frac{1}{2}\left(\frac{l}{r} - \frac{r}{l}\right)\phi. \quad (4)$$

Here, we use the approximation $\theta_l \sim -z_2/l - z_2^3/6l^3$. In these expressions, the terms that include z^3 are minute, because $z \ll 1$. Typical z values are on the order of 10^{-2} . These terms reflect the thicknesses and aberration effects of the mirrors. When terms including z^3 are neglected, $|\phi_3|$ becomes larger than $|\phi|$ by a factor $r/l > 1$, while $|z_3|$ becomes smaller than z by a factor $l/r < 1$. Thus, one may expect $z_1 > |z_3| > |z_5| > \dots$. After several reflections between the mirrors, however, the terms including z^3 become significant, as shown below. Using Eqs. (3) and (4), ϕ_3 and z_3 can be derived from ϕ and z . Therefore, these equations form a recursive set. The general formulae for ϕ_{2n-1} and z_{2n-1} are

$$\phi_{2n-1} = (-1)^n P_{2n-1}(x)z^3 + (-x)^{1-n}\phi, \quad (5)$$

$$\hat{z}_{2n-1} = (-x)^{n-1}z + \frac{1}{2}(-1)^n P_{2n-1}(x)z^3 + \frac{1}{2}(-1)^n (x^{n-1} - x^{1-n})\phi, \quad (6)$$

$$P_{2n-1}(x) = \left(\sum_{i=0}^{4n-7} x^{1-n+i} \right) - \left(\sum_{i=0}^{n-3} x^{4-n+4i} \right) - \left(\sum_{i=0}^{n-3} x^{3-n+4i} \right), \quad (7)$$

where $x \equiv l/r < 1$. During the initial phase, while the transit number is small, $|\hat{z}_{2n-1}|$ decreases with increasing n . However, Eq. (6) includes x^{1-n} , so this term becomes significant for large n . As a result, $|\hat{z}_{2n-1}|$ increases with n once n exceeds a certain number. Figure 3 shows an example of z_{2n-1} as a function of n . Here, we assume a configuration with the following parameters: $f_1 = r/2 = 762$ mm, $f_2 = l/2 = 508$ mm, $L = f_1 + f_2 = 1270$ mm, $z_1 = 35$ mm, and $\phi_1 = 0.32$ mrad. These parameters are chosen to duplicate the experiment described below. In Fig. 3, z_{2n-1} calculated by Eq. (6) and that calculated by a ray tracing code are plotted. This code tracks a ray with a given starting position and vector. When the ray hits one of the spherical mirrors, it is reflected according to the law of reflection. The z -coordinates of the reflection points are compared with the results of the analytical expression. The difference between the values obtained by Eq. (6) and the code is as small as 0.3% when $2n - 1 = 25$. $|z_{2n-1}|$ exhibits a minimum at around $2n - 1 = 13$.

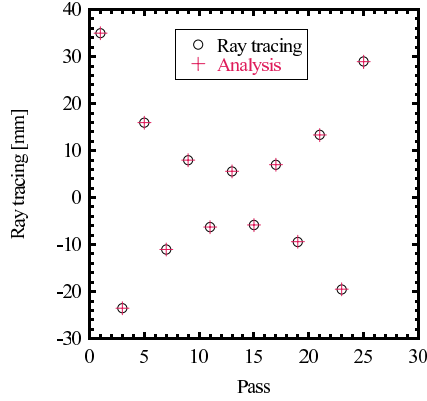


Fig. 3 Hit positions for each transit number $2n - 1$ derived by the analytic formula (+) and a ray tracing code (circles).

Considering $x < 1$, Eq. (6) for large n can be approximated by the leading term

$$\hat{z}_{2n-1} = \frac{1}{2}(-1)^n x^{1-n} (z^3 - \phi), \quad (8)$$

because this term includes x^{1-n} . Note that the next leading term, which includes x^{2-n} , becomes important when $z^3 \sim \phi$. Given the size of the first mirror, we can express the maximum transit number for this confocal mirror system. The radius of the first mirror should be larger than z_1 . We define the maximum transit number as the largest $2n - 1$ satisfying $|\hat{z}_{2n-1}| < z$. Hereafter, the maximum transit number is referred to as $2N_{\max} - 1$. Taking the logarithm of Eq. (8), N_{\max} is

$$N_{\max} = 1 + \frac{\log(2z/|z^3 - \phi|)}{|\log(x)|}. \quad (9)$$

When $z^3 = \phi$, we cannot use approximation (8), and we should extract the terms that include x^{2-n} from Eq. (6). Then, the expression for N_{\max} is

$$N_{\max} = 2 + \frac{\log(2/z^2)}{|\log(x)|}. \quad (10)$$

As we remove the x^{1-n} term by setting $z^3 = \phi$, we can remove the x^{2-n} term by adjusting ϕ . In this way, N_{\max} can be infinity. However, the difference between the optimum ϕ and $\phi = z^3$ is very small and finite errors in L and ϕ may reduce the maximum transit number. The results of the detailed analysis on the effects of errors in L and ϕ are described below. Equations (9) and (10) show that z should be small, $r/l = 1/x$ should be close to 1, and ϕ should be close to z^3 in order to obtain a large N_{\max} . Figure 4 shows a photograph of the first mirror of the confocal mirror system with the same parameters as the example described above. We used a He-Ne laser. Reflection spots are visible in the photograph. After 21 transits, the beam diameter increases to more than 40 mm and the spot becomes faint; hence, it becomes impossible to identify

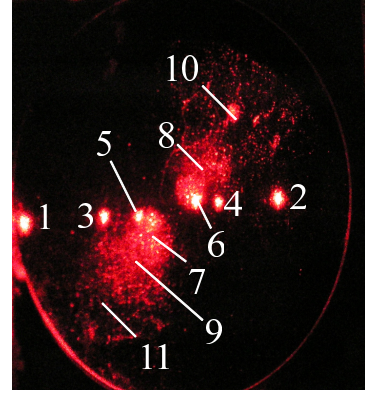


Fig. 4 Photograph of the first mirror of the confocal mirror system. Hit spots are numbered sequentially from 1 to 11.

further reflections. Although we used two convex lenses to suppress the beam expansion, the spot size increases. We will discuss this phenomenon later. The positions of the reflection spots agree with the results of analytic expression (6) within the margin of reading error. In this experiment, we set $\phi_1 = 0.32$ mrad in order to compare the experiment and the analytic formula. By adjusting the angle, the experimentally obtained maximum transit number was 28, whereas the maximum transit number was 43 at $\phi = 0$ using formula (9). The difference is partly due to difficulties in identifying reflection spots, as the beam becomes faint after a few tens of transits. Another reason for the difference is the effect of positioning and alignment errors. These effects are described below.

In practice, these errors cannot be ignored, and they may significantly modify Eqs. (5) and (6) and N_{\max} . Since the effect of angular error is already included in ϕ , we describe here the effect caused by the difference $\epsilon \equiv L - f_1 - f_2$. As in the preceding analysis, we keep the terms of $O(z^3)$ and neglect the higher-order terms. We assume $\phi = O(z^3)$ and $q = O(z^2)$, where $q \equiv \epsilon/l$ is the normalized difference. Replacing L with $L + \epsilon$, the modified ϕ_{2n-1} and z_{2n-1} are

$$\phi_{2n-1} = \frac{4q}{1-x^2} [(-x)^{n-1} - (-x)^{1-n}]z + (-1)^n P_{2n-1}(x)z^3 + (-x)^{1-n}\phi, \quad (11)$$

$$\hat{z}_{2n-1} = \{(-x)^{n-1} + \frac{2xq}{1-x^2} [(-x)^{n-1} - (-x)^{1-n}]\}z + \frac{1}{2}(-1)^n P_{2n-1}(x)z^3 + \frac{1}{2}(-1)^n (x^{n-1} - x^{1-n})\phi. \quad (12)$$

Equations (11) and (12) include new terms proportional to qz , which do not appear in Eqs. (5) and (6). From these formulae, the modified maximum transit number $2N_{\max} - 1$ is derived as

$$N_{\max} = 1 + \frac{\log(2z/|z^3 - \phi + \frac{4xq}{1-x^2}z|)}{|\log(x)|}. \quad (13)$$

We extract the terms including x^{1-n} as before. The additional term $4xqz/(1-x^2)$ appears, which do not appear in Eq. (9). Equation (13) indicates that z and q should be small, $r/l = 1/x$ should be close to 1, and ϕ should be close to z^3 in order to obtain a large N_{\max} . In practice, N_{\max} is often limited by positioning and alignment errors, which are expressed by q and a finite difference in ϕ from the optimum value.

In a practical system, the beam has a finite size, and the second mirror should be small enough not to cut the incident beam propagating toward the first mirror. This condition imposes a maximum limit on ($x < 1$); thus, we cannot choose x very close to one. Obviously, $z_2 \approx (-xz_1)$ should be larger than the beam radius. Furthermore, the window sizes of the laser injection and exit ports must be larger than z_1 . Therefore, z_1 and x must be chosen to satisfy these experimental conditions. $L = (f_1 + f_2)$ is the distance between the mirrors, which should be larger than the plasma size, so that the mirrors are located outside the plasma. In addition, in order to distinguish the forward- and backward-scattered signals, L should be large enough to separate these signals in the time domain.

Here, we discuss the mechanism of beam expansion, which can be seen in Fig. 4. The effects of aberration, surface roughness, and diffraction can cause beam expansion. First, we estimate the effect of aberration by using Eq. (12). By linearizing the final position z_{2n-1} with respect to the deviation in the initial condition $\delta z_1, \delta\phi$, we can estimate the beam expansion. The final beam diameter D_a is

$$D_a = 2 \left| \frac{\partial \hat{z}_{2n-1}}{\partial z} \delta z + r \frac{\partial \hat{z}_{2n-1}}{\partial \phi} \delta \phi \right|. \quad (14)$$

Substituting $\delta z_1 = 2.5$ mm, $\delta\phi_1 = 0.7$ mrad and $\epsilon = 15$ mm, D_a becomes 39 mm after 21 transits. Here, δz_1 is the initial beam radius and $\delta\phi_1$ is the beam divergence of the incident laser light under the experimental conditions. We used the terms that include x^{1-n} and x^{2-n} , because they are dominant in the present configuration. Second, we estimate the effect of angular scattering of the rays due to the surface roughness of the mirror. If the angular error generated at the $(2i-1)$ th reflection is denoted by θ_{2i-1} , the $(2n-1)$ th normalized position of the beam spot \hat{z}'_{2n-1} is

$$\begin{aligned} \hat{z}'_{2n-1} &= \hat{z}_{2n-1} + \sum_{i=2}^{n-1} \frac{\theta_{2i-1}}{2} (-1)^{n-i+1} (x^{n-i} - x^{i-n}) \\ &\approx \hat{z}_{2n-1} + \frac{\theta_3}{2} (-1)^n x^{2-n}, \end{aligned} \quad (15)$$

where \hat{z}_{2n-1} is the ideal position calculated by Eq. (12). θ_3 is the dominant term because $x < 1$ and θ_1 can be made zero by adjusting the initial angle ϕ_1 . When the surface roughness (i.e., deviation from a sphere) is $\lambda/4$, the corresponding θ is less than 0.01 mrad and the resultant beam diameter is $D_r < 0.3$ mm. Thus, this effect is negligible. Third, we estimate the effect of diffraction assuming a Gaussian beam. The formulae for Gaussian beam imaging

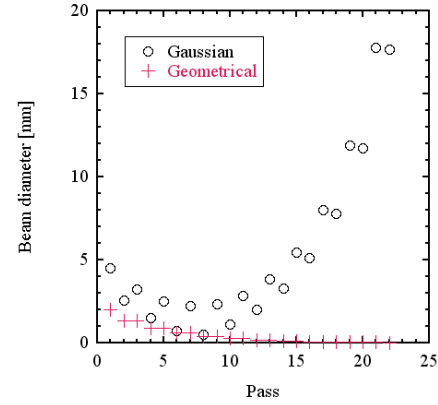


Fig. 5 Spot size on the mirrors for each transit number $2n-1$ assuming a Gaussian beam. $f_1 = 762$ mm, $f_2 = 508$ mm, $\epsilon = 0$ mm, $d_1 = 10,000$ mm, and $w_1 = 1$ mm.

by using an optical component with a focal length f are

$$d_2 = \frac{\left(\frac{\pi w_1^2}{\lambda}\right)^2 \frac{1}{f} - d_1 \left(1 - \frac{d_1}{f}\right)}{\left(\frac{\pi w_1^2}{\lambda}\right)^2 \left(\frac{1}{f}\right)^2 + \left(1 - \frac{d_1}{f}\right)^2}, \quad (16)$$

$$\left(\frac{w_2}{w_1}\right)^2 = \frac{1}{\left(\frac{\pi w_1^2}{\lambda}\right)^2 \left(\frac{1}{f}\right)^2 + \left(1 - \frac{d_1}{f}\right)^2}. \quad (17)$$

Here, d_1 and d_2 are the anterior and posterior focal lengths, respectively, and w_1 and w_2 are the waist sizes at these focal points. Since the initial injected beam is nearly collimated, $d_1 \gg f$ and $w_1 \gg \lambda$. After the first reflection, the beam has a waist near the focal point of the confocal mirror system. After the second reflection, the beam is nearly collimated. These initial behaviors are similar to those in geometrical optics. However, the Gaussian beam shows different behavior after several transits. Figure 5 shows the calculated spot size on the mirrors. The configuration parameters are as follows: $f_1 = 762$ mm, $f_2 = 508$ mm, the initial anterior focal length is $d_1 = 10,000$ mm, $w_1 = 1$ mm, and $\epsilon = 0$. When we consider a finite error in the distance between the mirrors, $\epsilon = -30$ mm, the spot diameter after 21 transits is about $D_d = 34$ mm. Therefore, both aberration and diffraction can cause beam expansion.

We present as an example the confocal spherical mirror system design for multi-pass Thomson scattering in the QUEST spherical tokamak device [3]. The radius of the vacuum vessel is 1.4 m. However, we choose $L = 5500$ mm. With this L , forward- and backward-scattered signals are separated by about 20 ns, which is sufficient for a fast detection system [4]. To pass a laser beam with a diameter of 8 mm, we choose the following parameters: mirror radii $D_1 = 50$ mm, $D_2 = 42$ mm; focal lengths $f_1 = 3100$ mm, $f_2 = 2400$ mm, and $z_1 = 21$ mm ($z = 3.39 \times 10^{-3}$); and $\phi = 0$. In this case, the maximum transit number $2N_{\max} - 1 = 95$ by using Eq. (9). To ensure a transit number of more than 40, the allowable position-

ing and alignment errors are $|\epsilon| < O(z^2) \times l \approx 0.06$ mm and $|\phi| < 4.5 \times 10^{-5}$ rad from Eq. (13). For large $\epsilon \approx O(z) \times l$, the approximate expression (13) cannot be applied. Using Eq. (12), the allowable positioning error is $|\epsilon| < 7.4$ mm (in contrast, using Eq. (13), the allowable positioning error is $|\epsilon| < 8.4$ mm). When we take parameters $d_1 = 10,000$ mm and $w_0 = 5$ mm, the beam diameter expands to $D > 40$ mm owing to diffraction. Therefore, the maximum transit number for practical conditions will be about 37.

In summary, the feasibility of multi-pass laser optics consisting of two confocal spherical mirrors has been studied. We obtained analytic expressions for the path and the maximum transit number, ϕ_{2n-1} , z_{2n-1} , and $2N_{\max} - 1$. The effects of aberration, positioning and alignment errors, and beam expansion are considered. An example of a confocal spherical mirror system design was described. In the

example, the maximum transit number can be more than 37, considering typical positioning and alignment errors and beam expansion.

This study was supported by Japan Society for the Promotion of Science (JSPS) Grant-in-Aid for Scientific Research No. 21246137 and National Institute for Fusion Science (NIFS) Collaborative Research Program No. NIFS09KUTR039.

- [1] A. Ejiri *et al.*, Nucl. Fusion **49**, 065010 (2009).
- [2] M. Yu. Kantor *et al.*, Plasma Phys. Control. Fusion **51**, 055002 (2009).
- [3] K. Hanada *et al.*, IEEJ Trans. FM **129**, 589 (2009).
- [4] A. Ejiri *et al.*, to be published in Plasma Fusion Res. Special Issue (ITC-19).